

Enhanced photovoltaic characterization of TiO₂ nanoparticle/nanotube composite film based on dye-sensitized solar cells and charge-transport mechanism discussion

C. KANG, Y. XIE, E. XIE*

School of Physical Science and Technology, Lanzhou University, Lanzhou 730000, People's Republic of China

We synthesized a TiO₂-based nanotubes/nanoparticles composite structural film (NPNT film) using monodispersed nanotubes by doctor blade technique. The monodispersed nanotubes were prepared by potentiostatic anodization of Ti foil with subsequent ultrasonic dispersing. For a comparison, TiO₂ nanoparticle film (NP film) and nanotube film (NT film) were also prepared in the same way. The NPNT film obtained obvious improved fill factor (FF) and total energy conversion efficiency (η) compared to traditional NP film. Charge-transport mechanism in NPNT film are discussed: The introduced nanotube is used as "electron expressway" for high-speed electron transport, which decrease electron transport resistance and thus produce markedly enhanced FF and improved total energy conversion efficiency.

(Received April 12, 2011; accepted May 31, 2011)

Keywords: TiO₂; Nanoparticle, Nanotube, Doctor-blade technique, Dye-sensitized solar cells

1. Introduction

Dye-sensitized solar cells (DSSCs) have attracted great interest in academic research and industrial applications owing to their higher efficiency and potentially lower cost compared to traditional silicon solar cells [1–4]. As one of the most important part of DSSCs structure, photoanode has been investigated with great enthusiasm for pursuing more suitable morphology and more excellent structure to improve DSSC efficiency. It is now well accepted that a high-efficiency photoelectrode for DSSC requires not only a large surface area for the loading of large amounts of dye molecules but also an ordered structure such as nanowires, nanotubes for fast electron transport [5, 6]. As is known, the TiO₂ nanoparticle film (NP film) can provide a rather large surface area for dye absorption but electron losses in transport is huge [7–9]. While the TiO₂ nanotube film (NT film) possesses higher electron-transport capability and stronger light-scattering property [10–12]. However, the specific surface area of the NT film is much smaller than the NP film resulting in an undesired reduction in the dye molecule adsorption [13, 14]. Therefore, the TiO₂ nanotubes/nanoparticles composite film (NPNT film) with combined advantages of NP film and NT film have been developed as a photoanode for DSSCs [15, 16].

Although the improved energy conversion efficiencies have been gained from various composite film DSSCs, however, the electron transport mechanism in NPNT film are still needed further investigation. Compared to nanotubes synthesized by hydrothermal methods, the anodized nanotubes are longer, have larger interior

diameter for dye-absorbed, and stronger mechanical properties not easily for collapse [17–19]. In our work, the anodized nanotubes have been used as the raw material to prepare NT film and NPNT film. Three kinds of film including NP film, NT film and NPNT film were prepared by doctor blade technique. The photovoltaic performance and total energy conversion efficiency of these three films have been tested. The NPNT film shows obvious enhanced FF and total energy conversion efficiency. The charge-transport mechanisms in NPNT film has been discussed.

2. Experimental

2.1. Preparation of TiO₂ nanotubes and nanoparticles

Ti foils with thickness of 220 μm were cleaned by sequential ultrasonic rinses in deionized water, acetone and ethanol for 20 min each. Then the cleaned Ti foils were subjected to potentiostatic anodization in a two-electrode electrochemical system which was connected to a potentiostatic DC power supply. Meanwhile, a 0.25 wt% NH₄F contained ethylene glycol solution was used as electrolyte and a Ti foil was used as counter electrode. Anodization was performed at 50 V for 17 hours under stirring. Finally, we obtained highly ordered TiO₂ nanotube arrays which would be used in the following section. In addition, TiO₂ nanoparticles were obtained from a commercially available TiO₂ powder (P25, Degussa).

2.2. Preparation of TiO₂ electrode and the assembly of DSSCs

Prior to fabricate TiO₂ electrode, fluorine-doped tin oxide coated glass (FTO, NSG, 2.2 mm in thickness, 14 Ω/square, 90+% transmittance in visible region) was cleaned ultrasonically in deionized water, acetone and ethanol for 20 min each.

The nanoparticle paste was prepared by grinding 1.0 g P25 under acetic acid in an agate mortar for 30 min. During the grinding process, about 1.5 mL acetic acid was added drop by drop to prevent the TiO₂ particles from aggregation. Then 2 ml deionized water was added drop by drop during grinding. Subsequently, the resulted suspension was added into a solution of 0.03 g PVP, 1ml ethanol and 0.5 ml acetic acid under strong stirring and ultrasonic dispersing. The nanotube paste was prepared in the same way but replacing P25 with anodized nanotubes. The composite paste was prepared by grinding a community of anodized nanotubes and P25 (weight ratio of 1:10). The three TiO₂ pastes were deposited onto cleaned FTO glasses by doctor blade technique. The thickness of the three films were controlled to be 20 μm.

All the films were sintered at 450 °C for 3h, then were soaked in 40 mM TiCl₄ aqueous solution at 70°C for 0.5 h, followed by sintering at 500 °C for 0.5 h. At 80 °C in the cooling, the TiO₂ electrodes were immersed into a 0.3mM solution of N-719 dye in a mixture of tert-butyl alcohol and acetonitrile (volume ratio of 1:1) for 24 h at room temperature to complete the sensitizer uptake. Then the dye-adsorbed TiO₂ electrode and the platinized counter electrode (5 mM H₂PtCl₆ in isopropanol, heated at 400 °C on FTO for 15 min) were assembled into a sandwich-type cell with the interior space filled with electrolyte (acetonitrile solution containing 0.05 M of I₂, 0.1 M of LiI and 0.5 M of 4-tert-butylpyridine) The effective area of the three cells was controlled to be 0.25 cm².

The morphologies and thicknesses of samples were characterized by Field emission scanning electron microscopy (FE-SEM) (Hitachi, S-4800). The structural properties of the films were studied by X-ray diffraction (XRD) (Philips X'pert Pro MPD, Cu Kα, 0.154056 nm). Photocurrent-voltage curves were measured under simulated solar light (AM 1.5, 100 mW/cm²).

3. Results and discussion

3.1. Morphological and structural characterization

Fig. 1a and 1b show the top-surface and cross-section views of as-prepared TiO₂ nanotube by anodization. These tube products have an highly ordered structure with an average diameter of 100 nm, tube wall of 10 nm and tube length of 20~30 μm (seen from the inset of Fig. 1b). Fig. 1c, 1d and 1e show the top-surface views of the NP film,

the NT film, and the NPNT film, respectively. As shown in Fig. 1c, the NP film is composed of nanoparticles with sizes from 10 nm to 50 nm. Fig. 1d shows the image of NT film, we can note that the nanotubes in NT film are in monodispersed disorderly state and the morphology of the nanotubes is in agreement with as-prepared samples (Fig. 1a and Fig. 1b). The NPNT film is a composite community with a few nanotubes embedded in NP film (Fig. 1e), in which the nanotubes and the nanoparticles combined with each other very well.

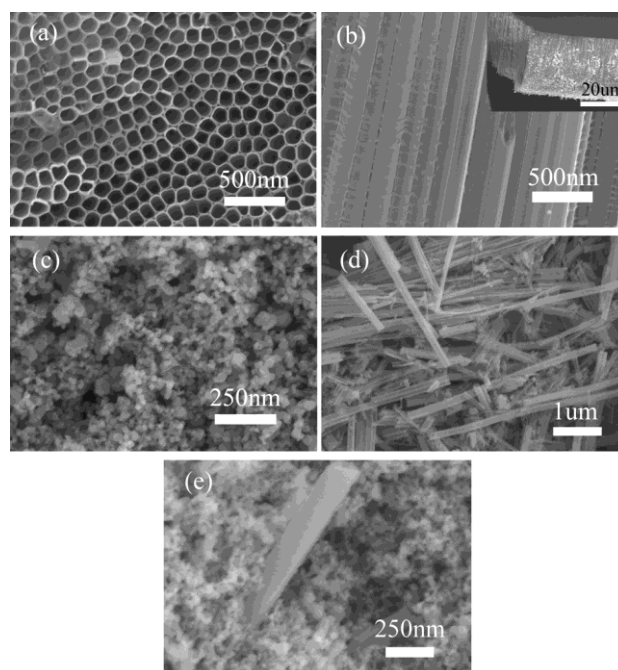


Fig. 1. FESEM images of top-surface view (a), cross-sectional view (b), and overall view in the inset of (b) of as-prepared nanotube grown by potentiostatic anodization; and the top-surface views of NP film (c), NT film (d) and NPNT film (e) after annealing, respectively.

Fig. 2a shows the XRD patterns of NP film, NT film and NPNT film after annealing at 450 °C in air. The peaks of (101), (004), (200), (105) and (211) are typical peaks of anatase TiO₂ [JCPDS: PDF#21-1272]. The peak of 2θ=51.3° comes from FTO substrate [JCPDS: PDF#30-1375]. As shown in Fig. 2a, all the three films exhibit highly crystallized anatase structure without any impurity phase. As a comparison, the XRD patterns of as-prepared NT film are also showed in Fig. 2b and an amorphous phase is displayed.

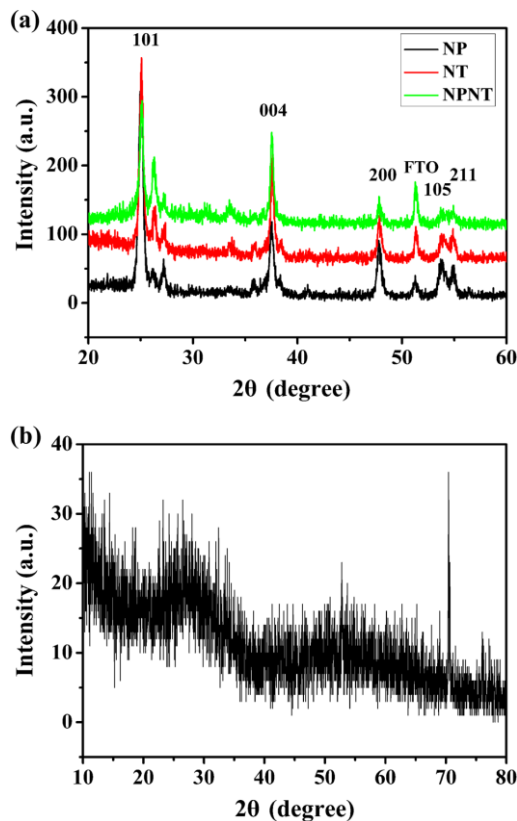


Fig. 2. XRD patterns of NP film, NT film, and NPNT film annealed at 450 °C in air (a) and as-prepared nanotube synthesized by potentiostatic anodization without annealing (b).

3.2. Photovoltaic performance

The photocurrent density–voltage curves (J – V curves) for DSSC based on NP film, NT film and NPNT film are shown in Fig. 3 and the corresponding values are summarized in Table 1. From Fig. 3 and Table 1, the NPNT film shows an improved total energy conversion efficiency of 4.96% which is 18.7% and 154% higher than the NP film (4.18%) and the NT film (1.95%), respectively. The improvement of the NPNT film is mainly ascribed to the improvement of short-circuit current density (J_{sc}) compared to NT film and the enhancement of fill factor (FF) compared to NP film. From the list of J_{sc} , the NPNT film shows a similar J_{sc} value with the NP film but much higher than NT film. This can be attributed to the closely-packed structure of NPNT film and NP film and the loosely-packed structure of NT film [20], which leads to larger specific surface areas of NPNT film and NP film than NT film. From Table 1, the FF of the NT film is the largest, next is the NPNT film, that of the NP film is the lowest, which may be related to interior transport resistance [16, 21]. As evidence, the interior electron transport mechanism of the three films are discussed below.

Table 1. The comparison of J_{sc} , V_{oc} , FF and the total efficiency (η) of NP film, NT film and NPNT film. All the measurements were performed under simulated solar light of AM 1.5 with light intensity of 100 mW/cm² and an effect area of 0.25 cm².

	J_{sc} (mA/cm ²)	V_{oc} (V)	FF	η
NP	12.8	0.673	0.485	4.18%
NT	4.52	0.674	0.64	1.95%
NPNT	12.6	0.681	0.578	4.96%

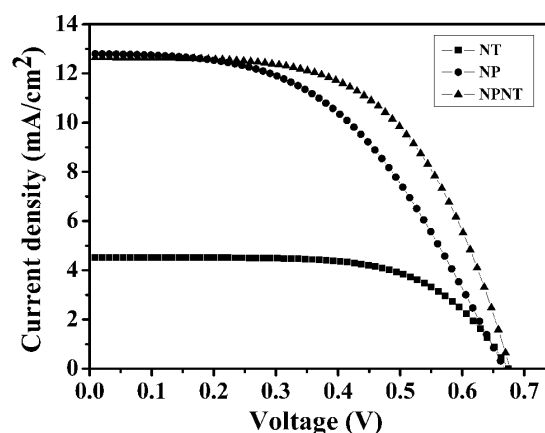


Fig. 3. J – V curves of DSSCs based on NP film, NT film and NPNT film.

3.3. Electron transport mechanism

Electron transport process in NP film and NT film is showed in Fig. 4a and 4b, respectively. As shown in Fig. 4a, electron transport in NP film is tortuous and often confront with dead end [22], which enormously increases the electron transport route. According to statistics data, electrons need experience over 1000 nanoparticles for transporting to collecting transparent conducting oxide (TCO) substrate [23, 24]. Besides, electrons transporting in NP film need cross grain boundary frequently. In this process, the surface states and potential barrier among nanoparticles increase largely the electron-recombination probability and transport-resistance among nanoparticles [25]. All these factors lead to the increase of the total internal transfer impedance. By contrast, in NT film, electrons can transport along the interior and exterior walls of nanotubes to the substrate (as shown in Fig. 4b). This is a route-saving and low electron-recombination probability way, which decreases electron-transport resistance and improves the electron-transport efficiency, in the name of electron expressway [26]. However, the loosely-stacking state of nanotubes result in the sharply decrease of the specific surface areas in NT film, in turn result in further decrease of J_{sc} .

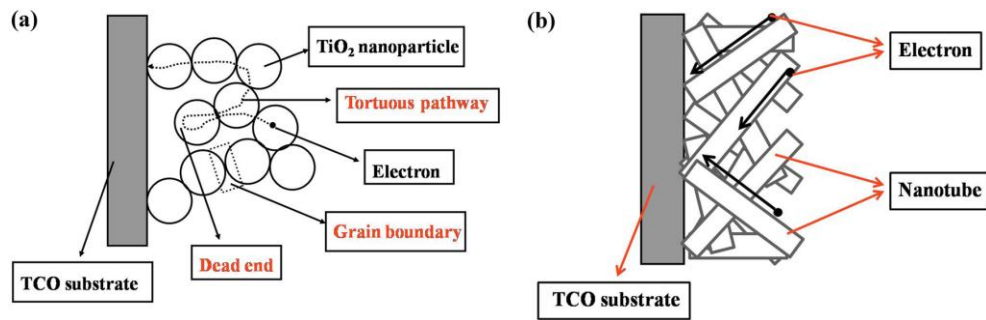


Fig. 4. Schematic diagram of electron-transport process in NP film (a) and NT film (b).

The electron transport process in NPNT film is shown in Fig. 5. The random walk of electrons [27] have much possibility to divert into the nanotube wall nearby and then transport along the nanotube wall (including the interior wall and the external wall) to the TCO substrate (shown in the magnifying part of Fig. 5). The electron transport process in NPNT film can be recognized as three stages: First, from nanoparticles to nanotubes via nanoparticles; second, along nanotubes; last, from nanotubes to substrate via nanoparticles. The first and last stages are carried out in nanoparticle network (process ① in Fig. 5). This process is tortuous but of short route. The second stage is carried out through the whole electrode (from front surface to back surface of electrode) (process ② in Fig. 5). This process is proceeded with the help of electron express-way (interior and exterior walls of nanotubes). Thus, this process is long-route but high-efficiency.

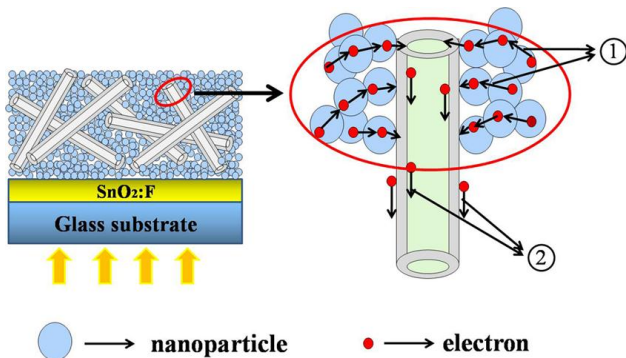


Fig. 5. Schematic diagram of structure of NPNT film and enlarged view of electron transport process in NPNT film. The electron-transport process in the first and last stages (①process) and the second stage (②process).

Supposing the resistances of these three stages are R_1 , R_2 , R_3 , and the corresponding electron transport lengths are l_1 , l_2 , l_3 , respectively. The total resistance of the whole process is R . Due to these three stages are proceeded one after another, the total resistance R of the whole process can be recognized as the tandem resistance of R_1 , R_2 and R_3 , described as follows:

$$R = R_1 + R_2 + R_3 \quad (1)$$

Where, the decision formula of R can be described as follows:

$$R = \sigma \frac{l}{s} \quad (2)$$

Supposing the electrons transport along a cross-section of fixed area (s). The transport distance l_1 and l_3 of the first and last stages are very small, so the transport resistance R_1 and R_3 are small as well. Hence, according to formula (1), the total transport resistance of the NPNT film can be mainly determined by R_2 . This explains that the NPNT film shows a slightly higher total resistance than NT film and thus a slightly lower FF than NT film. Further, as shown in Fig. 5, not only the transport distance l_2 of the second stage but also the transport resistance coefficient σ (defined as transport resistance per unit length) is much smaller than NP film, which results in the transport resistance of this stage (R_2) is much smaller than NP film. Due to the mainly transport process in NPNT film is carried out along nanotube, according to formula (1), the total transport resistance of NPNT film is mainly determined by R_2 , so the total transport resistance R of the whole transport process in NPNT film is also much smaller than NP film, which results in a much higher FF of NPNT film than that of NP film. Therefore, the whole transport process in NPNT film is low-resistant and high-efficiency, which leads to the increase of FF as confirmed by DSSC parameters.

On the other hand, the NPNT film possesses a similar specific surface area to NP film but higher than NT film, resulting in a similar J_{sc} of NPNT film and NP film but higher than NT film, which is consistent with J-V curve results. In a word, the charge-collection efficiency in NPNT film is improved significantly due to the nanotubes for electron transport expressway and nanoparticles for abundance of dye-adsorbed carrier.

4. Conclusions

In summary, we have successfully fabricated NPNT film using anodized nanotubes and investigated the photovoltaic characterization of the NPNT film based DSSC. Due to NPNT film combining the advantages of nanotube film (higher FF) and nanoparticle film (larger J_{sc}), the NPNT film based DSSC achieves great improvement with a total energy conversion efficiency of

4.96 %, which is 18.6% larger than NP film and is 1.5 times larger than NT film. Charge-transport mechanism in NPNT film is discussed, which explains the markedly improved FF of the NPNT film compared to that of the NP film. It is hopeful that the composite structure electrode will play larger potential superiority compared to single structure electrode and can be extended to other composite structure for improving the efficiency of DSSC.

Acknowledgements

This work is supported by NSAF Joint Funds of the National Natural Science Foundation of China (Grant No. 10776010) and partially by the Key Technology Research and Development Program of Gansu Province of China (Grant No. 1011GKCA027).

References

- [1] B. O'Regan, M. Grätzel, *Nature* **353**, 737 (1991).
- [2] M. Grätzel, *J. Photochem. Photobiol. C* **4**, 145 (2003).
- [3] M. Grätzel, *J. Photochem. Photobiol. A* **164**, 3 (2004).
- [4] A. Y. El-Etre, S. M. Reda, *Appl. Surf. Sci.* **256**, 6601 (2010).
- [5] M. Law, L. E. Greene, J. C. Johnson, R. Saykally, P. D. Yang, *Nat. Mater.* **4**, 455 (2005).
- [6] A. O. T. Patrocínio, E. B. Paniago, R. M. Paniago, N. Y. M. Iha, *Appl. Surf. Sci.* **254**, 1874 (2008).
- [7] K. Zhu, N. Kopidakis, N. R. Neale, J. van de Lagemaat, A. J. Frank, *J. Phys. Chem. B* **110**, 25174 (2006).
- [8] E. Enache-Pommer, J. E. Boercker, E. S. Aydil, *Appl. Phys. Lett.* **91**, 123116 (2007).
- [9] S. A. Haque, E. Palomares, B. M. Cho, A. N. M. Green, N. Hirata, D. R. Klug, J. R. Durrant, *J. Am. Chem. Soc.* **127**, 3456 (2005).
- [10] G. K. Mor, K. Shankar, M. Paulose, O. K. Varghese, C. A. Grimes, *Nano Lett.* **6**, 215 (2006).
- [11] H. Xu, X. Tao, D. T. Wang, Y. Z. Zheng, J. F. Chen, *Electrochim. Acta* **55**, 2280 (2010).
- [12] B. Tan, Y. Y. Wu, *J. Phys. Chem. B* **110**, 15932 (2006).
- [13] Y. Gao, M. Nagai, T. C. Chang, J. J. Shyue, *Cryst. Growth Des.* **7** 2467 (2007).
- [14] H. M. Cheng, W. H. Chiu, C. H. Lee, S. Y. Tsai, W. F. Hsieh, *J. Phys. Chem. C* **112**, 16359 (2008).
- [15] D. A. Wang, B. Yu, F. Zhou, C. W. Wang, W. M. Liu, *Mater. Chem. Phys.* **113**, 602 (2009).
- [16] X. D. Li, D. W. Zhang, S. Chen, Z. A. Wang, Z. Sun, X. J. Yin, S. M. Huang, *Mater. Chem. Phys.* **124**, 179 (2010).
- [17] M. Paulose, K. Shankar, S. Yoriya, H. E. Prakasham, O. K. Varghese, G. K. Mor, T. A. Latempa, A. Fitzgerald, C. A. Grimes, *J. Phys. Chem. B*, **110**, 16179 (2006).
- [18] M. Paulose, H. E. Prakasham, O. K. Varghese, L. Peng, K. C. Popat, G. K. Mor, T. A. Desai, C. A. Grimes, *J. Phys. Chem. C* **111**, 14992 (2007).
- [19] G. K. Mor, O. K. Varghese, M. Paulose, K. Shankar, C. A. Grimes, *Sol. Energ. Mat. Sol. C* **90**, 2011 (2006).
- [20] X. L. Sheng, N. R. Liu, J. Zhai, L. P. An, *Prog. Chem.* **21**, 1969 (2009).
- [21] T. Tesfamichael, G. Will, J. Bell, *Appl. Surf. Sci.* **245**, 172 (2005).
- [22] A. Hagfeldt, G. Boschloo, L. Sun, L. Kloo, H. Pettersson, *Chem. Rev.* **110**, 6595 (2010).
- [23] J. Bisquert, D. Cahen, G. Hodes, S. Rühle, A. Zaban, *J. Phys. Chem. B* **108**, 8106 (2004).
- [24] S. J. Chen, Y. C. Liu, C. L. Shao, R. Mu, Y. M. Lu, J. Y. Zhang, D. Z. Shen, X. W. Fan, *Adv. Mater.* **17**, 586 (2005).
- [25] K. D. Benkstein, N. Kopidakis, J. van de Lagemaat, A. J. Frank, *J. Phys. Chem. B* **107**, 7759 (2003).
- [26] Y. Suzuki, S. Ngamsinlapasathian, R. Yoshida, S. Yoshikawa, *Cent. Eur. J. Chem.* **4**, 476 (2006).
- [27] J. van de Lagemaat, A. J. Frank, *J. Phys. Chem. B* **105**, 11194 (2001).

*Corresponding author: xieeq@lzu.edu.cn